Molecular Tools for the Self-Assembly of Bisporphyrin Photodyads: A Comprehensive Physicochemical and Photophysical Study

Jérémy Brandel,[†] Ali Trabolsi,[†] Hassan Traboulsi,[†] Frédéric Melin,[‡] Matthieu Koepf,[‡] Jennifer A. Wytko,[‡] Mourad Elhabiri,*,[†] Jean Weiss,*,[‡] and Anne-Marie Albrecht-Gary*,[†]

Laboratoire de Physico-Chimie Bioinorganique, ULP-CNRS (UMR 7177), Institut de Chimie, ECPM, 25 Rue Becquerel, 67200 Strasbourg, France, and Laboratoire de Chimie des Ligands à Architecture Contrôlée, ULP-CNRS (UMR 7177), Institut de Chimie, 4 Rue Blaise Pascal, 67000 Strasbourg, France

Accessible and hindered phenanthroline-strapped Zn(II) porphyrin receptors exhibited suitable topography tailored to strongly and selectively bind N_1-unsubstituted imidazoles and imidazoles appended to free-base porphyrins. Distal binding was clearly driven by the formation of strong bifurcated hydrogen bonds with the phenanthroline unit of the receptors. An extensive physicochemical study emphasized the influence of bulkiness of the substrate and of the porphyrin receptor on the binding and self-assembly mechanism. Knowledge of the corresponding spectroscopic, thermodynamic, and kinetic data were of fundamental importance to elucidate and to model the photoinduced properties which occur within the self-assembled porphyrin dyads.

Introduction

In the search for photo- and electroactive materials, porphyrin assemblies exhibiting well-defined geometries and interactions, dyads, triads, or higher oligomers,[1,2] have been the focus of much attention over the past decades. Synthetic efficiency and processability requirements call for efficient but tunable self-assembly processes. Because the formation of discrete species is generally entropy favored in solution,[3] control of the assembly process during deposition on surfaces

is essential to the design of functional materials.[4−10] A large number of covalently associated donor−acceptor porphyrin dyads or extended assemblies have been designed to model

* To whom correspondence should be addressed. E-mail: elhabiri@chimie.u-strasbg.fr (M.E.), jweiss@chimie.u-strasbg.fr (J.W.), amalbre@chimie.u-strasbg.fr (A.-M.A.-G.).
† Laboratoire de Physico-Chimie Bioinorganique.
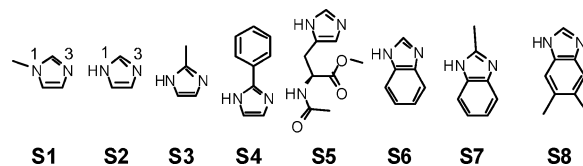‡ Laboratoire de Chimie des Ligands à Architecture Contrôlée.

(1) (a) Holten, D.; Bocian, D. F.; Lindsey, J. *Acc. Chem. Res.* **2002**, *35*, 57–69. (b) Harvey, P. D. In *The Porphyrin Handbook*; Kadish, K. M., Smith, K. M., Guilard, R., Eds.; Academic Press: San Diego, CA, 2003; Vol. 18, Chapter 113. (c) Wytko, J. A.; Weiss, J. In *N4-Macrocyclic metal complexes*; Zagal, J., Bedioui, F., Dodelet, J. P., Eds.; Springer: New York, 2006; Vol. 18, pp 63−250. (d) Kobuke, Y. *Struct. Bonding (Berlin, Ger.)* **2006**, *121*, 49−104.
(2) Winters, M. U.; Dahlstedt, E.; Blades, H. E.; Wilson, C. J.; Frampton, M. J.; Anderson, H. L.; Albinsson, B. *J. Am. Chem. Soc.* **2007**, *129*, 4291–4297, and references cited.
(3) (a) Lehn, J. M.; Rigault, A.; Siegel, J.; Harrowfield, J.; Chevrier, B.; Moras, D. *Proc. Natl. Acad. Sci. U.S.A.* **1987**, *84*, 2565–2569. (b) Fujita, M.; Tominaga, M.; Hori, A.; Therrien, B. *Acc. Chem. Res.* **2005**, *38*, 371–380. (c) Mathias, J. P.; Seto, C. T.; Simanek, E. E.; Whitesides, G. M. *J. Am. Chem. Soc.* **1994**, *116*, 1725–1736.

(4) (a) Subramanian, V.; Evans, D. G. *J. Phys. Chem. B* **2004**, *108*, 1085–1095. (b) Pullerits, T.; Sundstrom, V. *Acc. Chem. Res.* **1996**, *29*, 381–389. (c) Scholes, G. D.; Fleming, G. R. *J. Phys. Chem. B* **2000**, *104*, 1854–1868.
(5) (a) Wöhrle, D.; Schnurpfeil, G. In *The Porphyrin Handbook*; Kadish, K. M., Smith, K. M., Guilard, R., Eds.; Academic Press: San Diego, CA, 2003; Vol. 17, pp 177−246. (b) Collman, J. P.; Boulatov, R.; Sunderland, C. J. In *The Porphyrin Handbook*; Kadish, K. M., Smith, K. M., Guilard, R., Eds.; Academic Press: San Diego, CA, 2003; Vol. 11, pp 1−49. (c) Alessio, E.; Iengo, E.; Marzilli, L. G. *Supramol. Chem.* **2002**, *14*, 103−120. (d) Burrell, A. K.; Officer, D. L.; Plieger, P. G.; Reid, D. C. W. *Chem. Rev.* **2001**, *101*, 2751−2796. (e) Aratani, N.; Osuka, A. *Macromol. Rapid Commun.* **2001**, *22*, 725−740. (f) Balzani, V.; Ceroni, P.; Juris, A.; Venturi, M.; Campagna, S.; Puntoriero, F.; Serroni, S. *Coord. Chem. Rev.* **2001**, *219−221*, 545−572.
(6) Sanders, J. K. M. In *The Porphyrin Handbook*; Kadish, K. M., Smith, K. M., Guilard, R., Eds.; Academic Press: San Diego, CA, 2000; Vol. 3, pp 347−368.
(7) Imamura, T.; Fukushima, K. *Coord. Chem. Rev.* **2000**, *198*, 133−156.
(8) (a) Wojaczynski, J.; Latos-Grazynski, L. *Coord. Chem. Rev.* **2000**, *204*, 113−171. (b) Flamigni, L.; Barigelletti, F.; Armaroli, N.; Collin, J. P.; Dixon, I. M.; Sauvage, J. P.; Williams, J. A. G. *Coord. Chem. Rev.* **1999**, *190−192*, 671−682. (c) Tamiaki, H. *Coord. Chem. Rev.* **1996**, *148*, 183−197. (d) Kurreck, H.; Huber, M. *Angew. Chem., Int. Ed. Engl.* **1995**, *34*, 849−866. (e) Gribkova, S. E.; Evstigneeva, R. P.; Luzgina, V. N. *Russ. Chem. Rev.* **1993**, *62*, 963−979. (f) Gust, D.; Moore, T. A. *Top. Curr. Chem.* **1991**, *159*, 103−151.
(9) Gust, D.; Moore, T. A.; Moore, A. L. *Acc. Chem. Res.* **1993**, *26*, 198−205.
(10) Wasielewski, M. R. *Chem. Rev.* **1992**, *92*, 435−461.
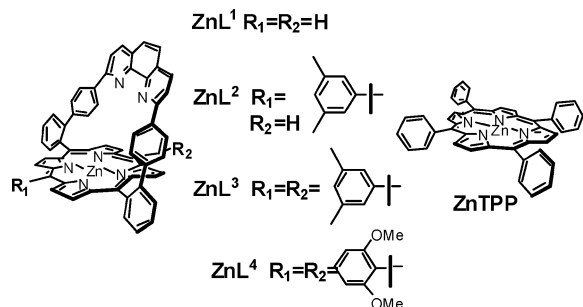
Figure 1. Chemical structures of the zinc porphyrin receptors.

Figure 2. Chemical structures of imidazoles and benzimidazoles **S1**–**S8**.

elementary recognition or communication events between building blocks.[9–11] In noncovalent assemblies of functional building blocks, the components are held together by multiple weak interactions such as metal–ligand coordination bonds, hydrogen bonds, electrostatic interactions, or hydrophobic forces. The efficiency and success of self-assembly are conditioned by the careful programming of the recognition patterns between building blocks. Like other applications of various strategies designed for efficient linear self-assembly,[12] multiporphyrins are mostly attained by multiple H-bonding, metal coordination, or a combination of both.[13,14] Inspired by the imidazole binding on zinc porphyrins as an assembling tool, we have taken advantage of both the selective recognition of imidazoles (Figure 1)[15,16] and the very efficient synthesis of phenanthroline superstructured porphyrins to design self-assembling supramolecular building blocks. We demonstrated that a careful ligand design based on the induced-fit principle led to the selective and strong recognition of imidazoles by the receptor (Figure 1). Imi-

dazole recognition results from a strong N-imidazolyl–Zn(II) axial coordination[6,7,8a,17] and bifurcated hydrogen bonds between the substrate and the nitrogen atoms of the 1,10-phenanthroline (noted phen) strap of the receptor. Moreover, introduction of secondary interactions (π–π stacking, CH–π, or hydrophobic interactions) may contribute to strengthen the final assemblies. This self-assembly approach was successfully implemented in photodyads[18] and linear porphyrin arrays.[19] Very recently, investigation of the self-assembly behavior of self-complementary building blocks showed that self-assembly guided via preferential weak interactions developed with a surface may compete with the classical entropy governed self-assembly in solution. As a result, drastic changes in the morphology of self-assembled species were observed, depending on a solution or a surface assembly mode.[20]

In the prospect of utilizing self-assembled porphyrin wires in prototypal devices, it is essential to fully control the parameters of the assembly process. Such control requires a careful assessment of all energetic parameters of the recognition process associated with the programmed assembly. We present herein an extensive physicochemical study of the recognition processes[21] of various substrates (Figures 2 and 3) by phen-strapped zinc(II) porphyrins Zn**L**^{1}–Zn**L**^{4} (Figure 1). In these receptors, meso-substitution by xylyl (Zn**L**^{2} and Zn**L**^{3}) or resorcinol-type (Zn**L**^{4})[22] groups offers the opportunity to study the influence of steric hindrance around the distal cavity. Imidazoles **S1**–**S5**, benzimidazoles **S6**–**S8**, and imidazole free-base porphyrins H$_2$**L**^{5} and H$_2$**L**^{6} were used to identify the key structural parameters controlling the

(11) (a) Gust, D.; Moore, T. A.; Moore, A. L. *Acc. Chem. Res.* **2001**, *34*, 40–48. (b) Holten, D.; Bocian, D. F.; Lindsey, J. S. *Acc. Chem. Res.* **2002**, *35*, 57–69. (c) Imahori, H. *J. Phys. Chem. B* **2004**, *108*, 6130–6143.

(12) (a) Frampton, M. J.; Anderson, H. L. *Angew. Chem., Int. Ed.* **2007**, *46*, 1028–1064. (b) Fages, F.; Wytko, J. A.; Weiss, J. *C. R. Chim.* **2008**, *11*, 1241–1253.

(13) (a) Weiss, J. *J. Inclusion Phenom. Macrocyclic Chem.* **2001**, *40*, 1–22. (b) Robertson, A.; Shinkai, S. *Coord. Chem. Rev.* **2000**, *205*, 157–199. (c) Ogoshi, H.; Hatakeyama, H.; Kotani, J.; Kawashima, A.; Kuroda, Y. *J. Am. Chem. Soc.* **1991**, *113*, 8181–8183. (d) Hayashi, T.; Miyahara, T.; Hashizume, N.; Ogoshi, H. *J. Am. Chem. Soc.* **1993**, *115*, 2049–2051.

(14) For recent examples of self-assembled porphyrin devices, see: (a) Nomoto, A.; Mitsuoka, H.; Oseki, H.; Kobuke, Y. *Chem. Commun.* **2002**, 1074–1075. (b) Nomoto, A.; Kobuke, Y. *Chem. Commun.* **2002**, 1104–1105. (c) Phillips-McNaughton, K.; Groves, J. T. *Org. Lett.* **2003**, *5*, 1829–1832. (d) Kuramochi, Y.; Satake, A.; Kobuke, Y. *J. Am. Chem. Soc.* **2004**, *126*, 8668–8669. (e) Takahashi, R.; Kobuke, Y. *J. Org. Chem.* **2005**, *70*, 2745–2753. (f) Furutsu, D.; Satake, A.; Kobuke, Y. *Inorg. Chem.* **2005**, *44*, 4460–4462. (g) Hwang, I. W.; Park, M.; Ahn, T. K.; Yoon, Z. S.; Ko, D. M.; Kim, D.; Ito, F.; Ishibashi, Y.; Khan, S. R.; Nagasawa, Y.; Miyasaka, H.; Ikeda, C.; Takahashi, R.; Ogawa, K.; Satake, A.; Kobuke, Y. *Chem.–Eur. J.* **2005**, *11*, 3753–3761. (h) Shoji, O.; Tanaka, H.; Kawai, T.; Kobuke, Y. *J. Am. Chem. Soc.* **2005**, *127*, 8598–8599. (i) Hajjaj, F.; Yoon, Z. S.; Yoon, M. C.; Park, J.; Satake, A.; Kim, D.; Kobuke, Y. *J. Am. Chem. Soc.* **2006**, *128*, 4612–4623. (j) Wytko, J. A.; Weiss, J. In *N4-Macrocyclic metal complexes*; Zagal, J., Bedioui, F., Dodelet, J. P., Eds.; Springer: New York, 2006; Vol. 18, pp 63–250. (k) Satakea, A.; Shojia, O.; Kobuke, Y. *J. Organomet. Chem.* **2007**, *692*, 635–644.

(15) Froidevaux, J.; Ochsenbein, P.; Bonin, M.; Schenk, K.; Maltese, P.; Gisselbrecht, J. P.; Weiss, J. *J. Am. Chem. Soc.* **1997**, *119*, 12362–12363.

(16) (a) Dharam, P.; Wytko, J. A.; Koepf, M.; Weiss, J. *Inorg. Chem.* **2002**, *41*, 3699–3704. (b) Dharam, P.; Melin, F.; Hirtz, C.; Wytko, J. A.; Ochsenbein, P.; Bonin, M.; Schenk, K.; Maltese, P.; Weiss, J. *Inorg. Chem.* **2003**, *42*, 3779–3787.

(17) (a) Iengo, E.; Zangrando, E.; Alessio, E. *Eur. J. Inorg. Chem.* **2003**, 2371–2384. (b) Wojaczynski, J.; Latos-Grażyński, L. *Coord. Chem. Rev.* **2000**, *204*, 113–171. (c) Heitz, V.; Chambron, J. C.; Sauvage, J. P. *The Porphyrin Handbook*; Kadish, K. M., Smith, K. M., Guilard, R., Eds.; Academic Press: New York, 2000; Vol. 6, pp 1–42. (d) Haycock, R. A.; Hunter, C. A.; James, D. A.; Michelsen, U.; Sutton, L. R. *Org. Lett.* **2000**, *2*, 2435–2438.

(18) Leray, I.; Valeur, B.; Paul, D.; Regnier, E.; Koepf, M.; Wytko, J. A.; Boudon, C.; Weiss, J. *Photochem. Photobiol. Sci.* **2005**, *4*, 280–286.

(19) Koepf, M.; Trabolsi, A.; Elhabiri, M.; Wytko, J. A.; Albrecht-Gary, A. M.; Weiss, J. *Org. Lett.* **2005**, *7*, 1279–1282.

(20) Koepf, M.; Wytko, J. A.; Bucher, J.-P.; Weiss, J. *J. Am. Chem. Soc.* **2008**, *130*, 9994–10001.

(21) (a) Fatin-Rouge, N.; Blanc, S.; Pfeil, A.; Rigault, A.; Albrecht-Gary, A. M.; Lehn, J. M. *Helv. Chim. Acta* **2001**, *84*, 1694–1711. (b) Hamacek, J.; Blanc, S.; Elhabiri, M.; Leize, E.; Van Dorsselaer, A.; Piguet, C.; Albrecht-Gary, A. M. *J. Am. Chem. Soc.* **2003**, *125*, 1541–1550. (c) Kalny, D.; Elhabiri, M.; Moav, T.; Vaskevich, A.; Rubinstein, I.; Shanzer, A.; Albrecht-Gary, A. M. *Chem. Commun.* **2002**, 1426–1427. (d) Elhabiri, M.; Hamacek, J.; Bünzli, J. C. G.; Albrecht-Gary, A. M. *Eur. J. Inorg. Chem.* **2004**, 51–62.

(22) Brandel, J.; Trabolsi, A.; Melin, F.; Elhabiri, M.; Weiss, J.; Albrecht-Gary, A. M. *Inorg. Chem.* **2007**, *46*, 9534–9536.
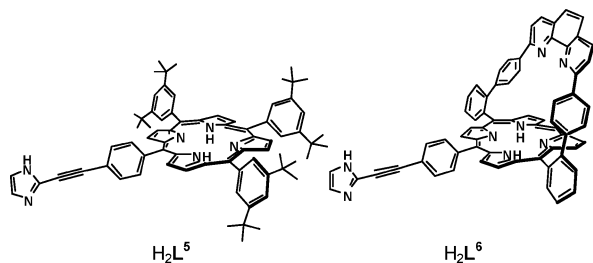
Figure 3. Chemical structures of the imidazole free-base porphyrins H_2L^5 and H_2L^6.

proximal/distal[23] recognition of these hosts. Knowledge of the spectroscopic, thermodynamic, structural, and kinetic data are fundamental prerequisites to examine the photoinduced processes of the dyads ZnL^i ($i = 1-4$) (Figure 1) and H_2L^5 or H_2L^6 (Figure 3).

Experimental Section

Solvents and Material. Zinc porphyrins, ZnL^1, ZnL^2, ZnL^3, ZnL^4, and $ZnTPP$ (TPP = tetraphenylporphyrin), were synthesized according to previously published procedures.[15,16,19,22,24] Imidazolyl free-base porphyrins H_2L^5 and H_2L^6 were synthesized according to a previously published procedure.[16a,19] The imidazole substrates (1-methyl-1H-imidazole **S1**, 1H-imidazole **S2**, 2-methyl-1H-imidazole **S3**, 2-phenyl-1H-imidazole **S4**, N-acetyl-L-histidine methyl ester **S5**, 1H-benzimidazole **S6**, 2-methyl-1H-benzimidazole **S7**, 5,6-dimethyl-1H-benzimidazole, **S8**) were purchased from commercial sources and used without further purification. All analyses were carried out with spectroscopic grade 1,2-dichloroethane (Merck, 99.8% or Carlo Erba, 99.8% for spectroscopy), which was further purified by distillation over CaH_2 to remove traces of HCl. All solutions were protected from daylight to avoid any photochemical degradation. All stock solutions were prepared using a AG 245 Mettler Toledo analytical balance (precision 0.01 mg), and the complete dissolution in 1,2-dichloroethane was achieved using an ultrasonic bath. The concentrations of the stock solutions of the receptors and substrates ($\approx 10^{-4}$ M) were calculated by quantitative dissolution of solid samples in 1,2-dichloroethane.

UV–Visible Titrations. The spectrophotometric titration of the receptors ZnL^i ($i = 1-4$; $\sim 10^{-5}-10^{-6}$ M) and $ZnTPP$ ($\sim 10^{-6}$ M) with S^n ($n = 1-8$), H_2L^5 and H_2L^6 were carried out in a Hellma quartz optical cell (1 or 2 cm). Microvolumes of a concentrated solution of S^n ($n = 1-8$), H_2L^5, or H_2L^6 were added to 4 mL (for $l = 2$ cm) or 2 mL (for $l = 1$ cm) of porphyrinic receptors with microliter Hamilton syringes (#710 and #750). Special care was taken to ensure that complete equilibration was attained. The corresponding UV–visible spectra were recorded from 290 to 700 nm on Kontron Uvikon 941 or Varian Cary 300 spectrophotometers maintained at 25.0(2) °C by the flow of a Haake NB 22 thermostat.

Luminescence Titrations. Luminescence titrations were carried out on solutions of ZnL^i ($i = 1-4$) or $ZnTPP$ with an absorbance smaller than 0.1 at wavelengths $\geq \lambda_{exc}$ in order to avoid any errors due to the inner filter effect. The titration of 2 mL (4 mL) of the metalloporphyrins was carried out in a 1 cm (2 cm) Hellma quartz optical cell by addition of known microvolumes of a solution of

S^n ($n = 1-8$), H_2L^5, or H_2L^6 with microliter Hamilton syringes (#710 and #750). The excitation wavelength corresponds to an isosbestic point (Soret band) between the free receptors and the pentacoordinated complexes or to the smallest absorbance amplitudes measured along the absorption spectrophotometric titrations. Besides, spectrofluorimetric variations of the $S_1 \rightarrow S_0$ transitions were monitored at absorbances <0.1 to minimize reabsorption processes. The zinc(II) porphyrin-centered luminescence spectra were recorded from 400 to 800 nm on a Perkin-Elmer LS-50B maintained at 25.0(2) °C by the flow of a Haake FJ thermostat. The light source was a pulsed xenon flash lamp with a pulse width at half-peak height <10 μs and power equivalent to 20 kW. The slit width was set at 15 nm for both the excitation and the emission.

Formation Kinetics. Formation kinetics of the pentacoordinated complexes (ZnL^i-S^n, $ZnL^i-H_2L^5$, and $ZnL^i-H_2L^5$, $i = 1-4$, $n = 3-8$) were investigated using an Applied Photophysics SX-18MV stopped-flow spectrophotometer with absorption and emission detection. The reactants were thermostated at 25.0(2) °C (Lauda M12 thermostat) and mixed in a 1 cm optical cell. Pseudo-first-order conditions with respect to imidazoles were used with imidazole concentrations at least 10 times higher than receptor concentrations. With absorption detection, the reaction was monitored at wavelengths corresponding to the largest amplitude (Soret band for ZnL^i-S^n). For fluorescence measurements with ZnL^i-S^n, the excitation monochromator slits were set at 3 nm, and the excitation wavelength corresponded to an isosbestic point (Soret or Q bands) between the free receptors and the pentacoordinated complexes. A 550 nm band-pass plastic-glass filter (transparent to light with $\lambda > 550$ nm, Schott KV550) was used for measuring the emitted light. Due to the fact that H_2L^5 or H_2L^6 substrates are also absorbing and light emitting species within the same spectral windows of the zinc porphyrins, a pair of band-pass filters ($\lambda > 550$ nm; Schott KV550) and interference filters ($\lambda < 660$ nm; IF660) is selected to isolate the emission bands of interest in the spectral region that allows the kinetics formation of the dyads to be monitored. The data sets, averaged out of at least three replicates, were recorded and analyzed with the commercial software Biokine.[25] This program fits up to three exponential functions to the experimental curves with the Simplex algorithm[26] after initialization with the Padé–Laplace method.[27] Variation of the pseudo-first-order rate constants with the analytical concentrations of reagents were processed using commercial programs (Origin 5.0[28]).

Activation Parameters. The temperature dependence of the formation kinetic was investigated for ZnL^i-S3 and ZnL^i-S4 complexes ($i = 1-4$). The experimental protocol described above was herein applied. Kinetic experiments were performed at temperatures ranging from 21.0 to 38.0 (error = ±0.2 °C). A Lauda cryostat (Ultra Kryomat TK30) was used as the cooling unit whereas a Lauda M12 thermostat was employed as the heating system. The poor solubility of the imidazoles at low temperature prevented the decrease of the temperature below 20 °C. Enthalpies and entropies of the reactions were calculated from conventional Eyring plots ($\ln(k/T) = f(1/T)$) using the Origin 5.0 program.[28]

Photophysical Studies. Emission spectra were collected on a Perkin-Elmer LS-50B luminescence spectrophotometer with solutions of absorbance less than 0.05 at a wavelength $> \lambda_{ex}$ in order to avoid any errors due to the inner filter effect. Absorption spectra were also measured along the fluorescence titration by using a Varian CARY 300 spectrophotometer. Fluorescence quantum yields

(23) For definition of distal and proximal binding sites, see: (a) Sage, J. T.; Champion, P. M. In *Small Substrate Recognition in Heme Proteins; Comprehensive Supramolecular Chemistry*; Suslick, K. S., Ed.; Pergamon Press: Oxford, U.K., 1996; Vol. 5, pp 171−213. (b) Momenteau, M.; Reed, C. A. *Chem. Rev.* **1994**, *94*, 659.

(24) Wytko, J. A.; Graf, J. E.; Weiss, J. *J. Org. Chem.* **1992**, *57*, 1015–1018.

(25) *Biokine*; Bio-Logic Company: Echirolles, 1991.

(26) Nelder, J. A.; Mead, R. *Comput. J.* **1965**, *7*, 308–313.

(27) Yeramian, E.; Claverie, P. *Nature* **1987**, *326*, 169–174.

(28) *Microcal Origin*; Microcal Software, Inc.: Northampton, MA, 1997.

Table 1. Spectroscopic and Photophysical Parameters of Zinc(II) Strapped Porphyrins ZnL^i ($i = 1-4$)[a]

	absorption λ^{max} (nm) [$\varepsilon^{\lambda max}$ ($\times 10^4$ M^{-1} cm^{-1})]			emission λ^{max} (nm)			
	$S_2 \leftarrow S_0$ B(0,0)	$S_1 \leftarrow S_0$		$S_1 \rightarrow S_0$			
L		Q(1,0)	Q(0,0)	Q(0,0)	Q(0,1)	Q_L^{abs} (%) [λ_{exc} (nm)]	τ (ns)
ZnTPP	419 (66)	548 (2.4)	585 (0.5)	599	647	3.3[c]	~2[c]
ZnL^1	419 (25)	549 (1.47)	586 (0.24)	594	646	1.6 (433[d], 550[e]); 2.3[b] (430)	2.2[b]
ZnL^2	424 (30)	550 (1.75)	585 (0.19)	601	648	0.9 (428[d], 550[e])	
ZnL^3	430 (55)	559 (1.83)	601 (0.52)	609	659	1.4 (422[d], 550[e])	
ZnL^4	434 (33)	564 (1.77)	604 (0.43)	611	664	1.5 (420[d], 550[e])	

[a] Solvent = 1,2-dichloroethane; T = 25.0(2) °C. [b] Reference 18. Solvent = dichloromethane; T = 25 °C. [c] References 30e, 41, and 42. Solvent = toluene; T = 25 °C. The uncertainties on the λ_{max}, $\varepsilon^{\lambda max}$, and Q_L^{abs} are 1 nm, 5%, and 30%, respectively. [d] λ_{exc} used with $(Ru(Bpy)_3)^{2+}$ as a reference. [e] λ_{exc} used with ZnTPP as a reference.

for zinc and free-base porphyrins were determined relative to two references, the fluorescent standard $(Ru(bpy)_3)^{2+}$ (tris[(2,2'-bipy-ridyl)ruthenium(II)] chloride hexahydrate (Φ = 0.028, air-equilibrated water), Strem Chemicals 98%) and the fluorescent ZnTPP (Φ = 0.033, toluene), with the possibility of correcting for differences between the refractive index of the reference n_r and the sample solutions n_s using the following expression:

$$Q_f(s) = Q_f(r)\frac{\int I_s(\lambda) \times A_r \times n_s^2}{\int I_r(\lambda) \times A_s \times n_r^2}$$

The indices s and r denote sample and reference, respectively. The integrals over I represent areas of the corrected emission spectra, and A is the optical density at the excitation wavelength.

Processing of the Spectrophotometric Data. The spectrophotometric data were processed with the Specfit programs, which adjust the stability constants and the corresponding extinction coefficients of the species formed at equilibrium. Specfit[36-38] uses factor analysis to reduce the absorbance matrix and to extract the eigenvalues prior to the multiwavelength fit of the reduced data set according to the Marquardt algorithm.[39,40] Distribution curves of the various species were calculated using the Haltafall program.[29]

Results and Discussion

Spectrophotometric Properties of the Free Porphyrin Receptors. The absorption spectra of free receptors ZnL^1-ZnL^4 exhibit the usual set[30] of bands for zinc(II) metalloporphyrins with a Soret (or χ) band centered at ~420 nm ($\varepsilon \approx 10^5$ M^{-1} cm^{-1}) and two Q (or α/β) bands ($\varepsilon \approx 10^4$ M^{-1} cm^{-1}) between 500 and 650 nm.[30a,d,31,32] The phen strap in receptors ZnL^i ($i = 1-4$) gives rise to an additional absorption band in the UV range between 260 and 375 nm.

In ZnL^1, the 2,9-diphenyl-1,10-phenanthroline strap induced significant hypochromic effects on the Soret and Q bands with respect to ZnTPP. This hypochromism could be due to classical electronic effects and geometrical constraints

in solution.[33] In contrast, in the solid state the X-ray structure of ZnL^1 revealed that no conformational restraints of the tetrapyrrolic macrocycle were imposed by the rigid strap.[15] The additional substitution of the two free meso-positions by one xylyl (ZnL^2), two xylyls (ZnL^3), and two 2,6-dimethoxyphenyl (ZnL^4) groups induced red shifts of the metalloporphyrin-centered transitions (Table 1). These shifts were attributed to electronic effects and porphyrin ring distortions caused by these substituents. Moreover, photoexcitation of the Soret transitions of the phen-strapped Zn(II) porphyrins resulted in two emission bands in the 600−700 nm spectral window. These emission bands were attributed to the $S_1 \rightarrow S_0$ (Q(0,0) and Q(0,1)) transitions (Table 1).[30-32]

Coordination of Imidazoles by ZnTPP. To evaluate the influence of the phen strap on the recognition properties of a series of imidazoles, it was essential to first consider a reference metalloporphyrin, ZnTPP (Figure 1), that possesses two identical faces. For ZnTPP complexes, the only interaction with imidazole is the strong N-Zn coordination.[34] Even though the binding properties of ZnTPP with various nitrogen bases have been reported,[35] for the sake of comparison, the stability of $ZnTPP-S^n$ ($n = 1-8$, Figure 2) and $ZnTPP-H_2L^6$ (Figure 3) were examined under our experimental conditions (1,2-dichloroethane, T = 25 °C). Absorption and emission titrations were conducted, and the corresponding thermodynamic parameters (Table 2) were calculated by statistical processing[36-40] of the data.

The stability constants mainly reflect electronic effects of the substituents on the N_3-heteroatom (Figure 2), which binds to zinc(II). The binding constants follow the order of the pK_a values that are tuned by substituent-induced electronic effects.[43,50] The similar values obtained for complexes $ZnTPP-S2$ and $ZnTPP-H_2L^5$ confirm the absence of steric

(29) Ingri, N.; Kakolowicz, W.; Sillen, L. G.; Warnqvist, B. *Talanta* **1967**, *14*, 1261–1286.

(30) (a) Gouterman, M. In *The Porphyrins*; Dolphin, D., Ed.; Academic Press: New York, 1978; Vol. 3, pp 1−165. (b) Dorough, G. D.; Miller, J. R.; Huennekens, F. M. *J. Am. Chem. Soc.* **1951**, *73*, 4315–4320. (c) Thomas, D. W.; Martell, A. E. *J. Am. Chem. Soc.* **1956**, *78*, 1338–1343. (d) Edwards, L.; Dolphin, D. H.; Gouterman, M.; Adler, A. D. *J. Mol. Spectrosc.* **1971**, *38*, 16–32. (e) Seybold, P. G.; Gouterman, M. *J. Mol. Spectrosc.* **1969**, *31*, 1–13.

(31) (a) Humphry-Baker, R.; Kalyanasundaram, K. *J. Photochem.* **1985**, *31*, 105–112. (b) Seely, G. R.; Calvin, M. *J. Chem. Phys.* **1955**, *23*, 1068–1078.

(32) Nappa, M.; Valentine, J. S. *J. Am. Chem. Soc.* **1978**, *100*, 5075–5080.

(33) (a) Haddad, R. E.; Gazeau, S.; Pécaut, J.; Marchon, J. C.; Medforth, C. J.; Shelnutt, J. A. *J. Am. Chem. Soc.* **2003**, *125*, 1253–1268. (b) Cramariuc, O.; Hukka, T. I.; Rantala, T. T. *J. Phys. Chem. A* **2004**, *108*, 9435–9441.

(34) Satake, A.; Kobuke, Y. *Tetrahedron* **2005**, *61*, 13–41.

(35) (a) Szintay, G.; Horvath, A. *Inorg. Chim. Acta* **2000**, *310*, 175–182. (b) Bhyrappa, P.; Krishnan, V.; Nethaji, M. *J. Chem. Soc., Dalton Trans.* **1993**, 1901–1906. (c) Vogel, G. C.; Stahlbush, J. R. *Inorg. Chem.* **1977**, *16*, 950–953. (d) Zaitseva, S. V.; Zdanovich, S. A.; Ageeva, T. A.; Golubchikov, O. A.; Semeikin, A. S. *Russ. J. Coord. Chem.* **2001**, *27*, 152–157.

(36) Gampp, H.; Maeder, M.; Meyer, C. J.; Zuberbühler, A. D. *Talanta* **1985**, *32*, 95–101.

(37) Gampp, H.; Maeder, M.; Meyer, C. J.; Zuberbühler, A. D. *Talanta* **1985**, *32*, 257–264.

(38) Gampp, H.; Maeder, M.; Meyer, C. J.; Zuberbühler, A. D. *Talanta* **1986**, *33*, 943–951.

(39) Marquardt, D. W. *J. Soc. Ind. Appl. Math.* **1963**, *11*, 431–441.

Table 2. Stability Constants of Imidazoles **S1**−**S8**, H$_2$**L**^{5}, and H$_2$**L**^{6} with Zn**L**^{1}−Zn**L**^{4} and Zn**TPP** Receptors[a]

	S1	S2	S3	S4	S5	S6	S7	S8	H$_2$L^5	H$_2$L^6
log $K_{ZnTPP-S}$	4.7(2)	4.5(1)	4.9(2)	2.54(6)	3.8(1)	4.34(6)	3.0(1)	4.6(1)		4.1(2)
log K_{ZnL1-S}	4.3(3)	5.9(1)	7.6(4)	3.92(7)	5.3(4)	5.8(4)	5.3(4)	5.69(9)	5.9(5)	6.0(4)
log K_{ZnL2-S}	3.6(1)	6.10(8)	7.0(2)	4.25(9)	5.1(1)	5.5(3)	5.50(6)	5.86(9)	5.8(2)	6.3(3)
log K_{ZnL3-S}	3.4(2)	6.1(1)	7.0(1)	4.10(7)	4.9(2)	4.9(4)	5.6(1)	5.69(7)	6.0(4)	6.1(4)
log K_{ZnL4-S}	3.6(1)	7.0(2)	7.7(5)	2.3(3)	5.14(4)	6.0(3)	6.14(9)	5.5(1)	5.2(4)	5.0(3)

[a] Solvent = 1,2-dichloroethane; T = 25.0(2) °C. Stability constants determined from UV−visible absorption and fluorescence spectrophotometric titrations (see Supporting Information). Uncertainties = 3σ, with σ the standard deviation.

interactions within the self-assembled bisporphyrin species (Table 2).

The electronic and relative fluorescence emission spectra of the Zn(II)-pentacoordinated species are given in Figures S1−S16 in the Supporting Information. Upon formation of the fifth coordination bond to the zinc atom, the $S_1 \leftarrow S_0$ and $S_2 \leftarrow S_0$ (Q and Soret bands, respectively)[30,41,44] and $S_1 \rightarrow S_0$ transitions[41c,d] showed significant and anticipated bathochromic shifts.[45−47] These characteristic spectral changes are mainly due to (i) the polarizability of the substrate, (ii) the strength of the *N*-axial coordination and the charge transfer, which mainly rely on the basicity of the substrate,[32,47−49] and (iii) the induced out-of-plane displacement of the metal center and deformation of the metalloporphyrin macrocycle.[50,51]

Coordination of Imidazoles by Strapped−Zn(II)-Porphyrin Zn L^1. Significant bathochromic shifts of the Soret and Q absorption bands ($\Delta\lambda$ > 10 nm, Figure 4)[22] were observed for the axial binding of the N_1-unsubstituted substrates **S2**−**S8** on Zn**L**^{1} (Figures S17−S32 in the Supporting Information).

(40) Maeder, M.; Zuberbühler, A. D. *Anal. Chem.* **1990**, *62*, 2220–2224.

(41) (a) Ohno, O.; Kaizu, Y.; Kobayashi, H. *J. Chem. Phys.* **1985**, *82*, 1779–1787. (b) Gurzadyan, G. G.; Tran-Thi, T. H.; Gustavsson, T. *J. Chem. Phys.* **1998**, *108*, 385–388. (c) Baskin, J. S.; Yu, H. Z.; Zewail, A. *J. Phys. Chem. A* **2002**, *106*, 9837–9844. (d) Yu, H. Z.; Baskin, J. S.; Zewail, A. *J. Phys. Chem. A* **2002**, *106*, 9845–9854.

(42) Strachan, J. P.; Gentemann, S.; Seth, J.; Kalsbeck, W. A.; Lindsey, J. S.; Holten, D.; Bocian, D. F. *J. Am. Chem. Soc.* **1997**, *119*, 11191–11201.

(43) Ogoshi, H.; Mizutani, T.; Hayashi, T.; Kuroda, Y. In *The Porphyrin Handbook*; Kadish, K. M., Smith, K. M., Guilard, R., Eds.; Academic Press: San Diego, CA, 2000; Vol. 6, pp 1−49.

(44) Gouterman, M. *J. Chem. Phys.* **1959**, *30*, 1139–1161.

(45) Wang, M. Y. R.; Hoffman, B. M. *J. Am. Chem. Soc.* **1984**, *106*, 4235–4240.

(46) Kirksey, C. H.; Hambright, P.; Storm, C. B. *Inorg. Chem.* **1969**, *8*, 2141–2144.

(47) (a) Antipas, A.; Dolphin, D.; Gouterman, M.; Jonhson, E. C. *J. Am. Chem. Soc.* **1978**, *100*, 7705–7709. (b) Quimby, D. J.; Longo, F. R. *J. Am. Chem. Soc.* **1975**, *97*, 5111–5117. (c) Caughey, W. S.; Fujimoto, W. Y.; Johnson, B. P. *Biochemistry* **1966**, *5*, 3830–3843.

(48) Wang, M. Y.; Rachel Hoffman, B. M. *J. Am. Chem. Soc.* **1984**, *106*, 4235–4240.

(49) Kirksey, C. H.; Hambright, P.; Storm, C. B. *Inorg. Chem.* **1969**, *8*, 2141.

(50) (a) Mc Dermott, G. A.; Walker, F. A. *Inorg. Chim. Acta* **1984**, *91*, 95–102. (b) Kadish, K. M.; Shiue, L. R. *Inorg. Chem.* **1982**, *21*, 3623–3630. (c) Kadish, K. M.; Shiue, L. R.; Rhodes, R. K.; Bottomley, L. A. *Inorg. Chem.* **1981**, *20*, 1274–1277. (d) Kadish, K. M.; Rhodes, R. K. *Inorg. Chem.* **1981**, *20*, 2961–2966. (e) Vogel, G. C.; Stahlbusch, J. R. *Inorg. Chem.* **1977**, *16*, 950–953. (f) Valentine, J. S.; Tatsuno, Y.; Nappa, M. *J. Am. Chem. Soc.* **1977**, *99*, 3522–3523. (g) Cole, S. J.; Curthoys, G. C.; Magnusson, E. A.; Phillips, J. N. *Inorg. Chem.* **1972**, *11*, 1024–1028.

(51) Wertsching, A. K.; Koch, A. S.; DiMagno, S. G. *J. Am. Chem. Soc.* **2001**, *123*, 3932–3939.
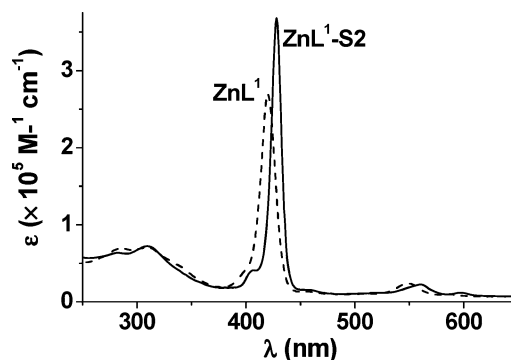
Figure 4. Electronic spectra of Zn**L**^{1} and its pentacoordinated complex with **S2**. Solvent = 1,2-dichloroethane; T = 25.0(2) °C.

Under our experimental conditions, the absorption band of 2,9-diphenyl-1,10-phenanthroline underwent spectrophotometric changes upon protonation (Figure S33 in the Supporting Information). Similar spectral changes were observed for distal[23] recognition of substrates **S2**−**S8** by Zn**L**^{1}. In contrast, the titration of Zn**L**^{1} with N_1-methylated **S1** led to very small bathochromic shifts of the Soret and Q bands ($\Delta\lambda$ = 2 nm), and no clear spectral variation of the phen-centered transitions was observed.[22] These spectrophotometric observations clearly demonstrate a proximal[23] recognition of **S1** by Zn**L**^{1}. For substrates H$_2$**L**^{5} or H$_2$**L**^{6}, the highly intense Soret bands limited the spectral window to the Q bands (Figure 5 and Figures S34−S37 in the Supporting Information).
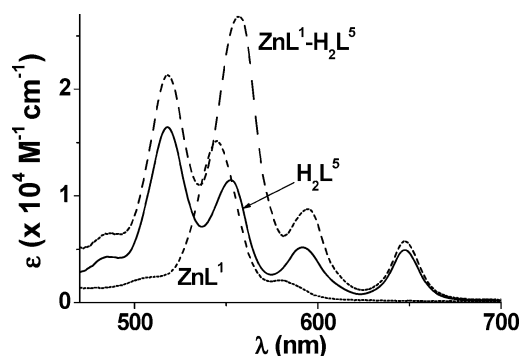
Figure 5. Electronic spectra of Zn**L**^{1}, of H$_2$**L**^{5}, and of the Zn**L**^{1}−H$_2$**L**^{5} complex. Solvent = 1,2-dichloroethane; T = 25.0(2) °C.

Statistical processing[36−38] of the spectrophotometric data supported the exclusive formation of 1:1 species corresponding to the axial ligation of a guest on the metallic center of Zn**L**^{1}, which is in agreement with the observation of distinct

(52) (a) Miller, J. R.; Dorough, G. D. *J. Am. Chem. Soc.* **1952**, *74*, 3977–3981. (b) Kirksey, C. H.; Hambright, P. *Inorg. Chem.* **1970**, *9*, 958–960.

isosbestic points.[47,52] The corresponding stability constants of the pentacoordinated complexes with ZnL^1 are given in Table 2. These thermodynamic data emphasized that N_1-unsubstituted substrates are stabilized by factors of 12 to 500 with respect to $ZnTPP$. In contrast, N_1-methyl-imidazole ($S1$) forms a less stable complex with ZnL^1 (log $K_{ZnL1-S1}$ = 4.3(3)) than with unstrapped $ZnTPP$ metalloporphyrin (log $K_{ZnTPP-S1}$ = 4.7(2)), in agreement with a proximal recognition process.

The stabilization for binding of substrates $S2-S8$, H_2L^5, and H_2L^6 within ZnL^1 originates from the presence of the phen strap, which is able to interact with substrates via bifurcated hydrogen bonds. Indeed, clear evidence for hydrogen bonding between the imidazole substrates and the two phen nitrogens was previously established by ^{1}H NMR and 2D ^{1}H NMR data in solution and X-ray diffraction in the solid state (ZnL^1-S2, ZnL^1-S3, ZnL^1-S4).[15,16b] The distances measured between the N_1H pyrrolic proton, which was accurately located by the presence of residual electronic density, and the two phen nitrogen atoms varied from 2.12 to 2.40 Å, thus confirming the presence of unsymmetrical bifurcated hydrogen bonds.[15,16b]

Our thermodynamic data revealed, in excellent agreement with the available X-ray structures and ^{1}H NMR studies,[15,16] that the apparently rigid Zn(II) porphyrin ZnL^1 was able to accommodate on its distal face[23] a series of bulky substrates as a result of porphyrin-ring distortion and the large tilt[15,16b] of the strap above the tetrapyrrolic plane (~10°). Complementary weak interactions (hydrogen bonds, $\pi-\pi$, and CH$-\pi$) between the substrates and ZnL^1 aid in stabilization compared with $ZnTPP$. In addition, these weak interactions likely compensate for the steric interactions due to bulkiness of the substrates and geometrical constraints of the porphyrin receptor induced upon the distal binding (Figure 6).
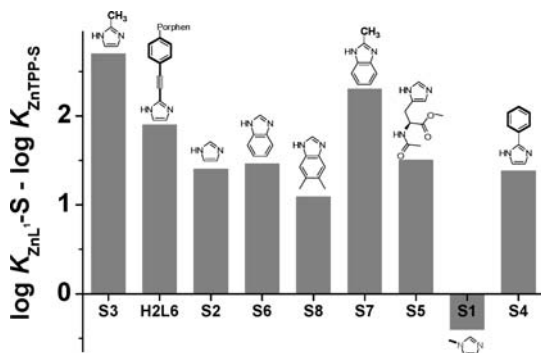

Figure 6. Difference in stability (log K_{ZnL^1-S} −log $K_{ZnTPP-S}$) of $S1-S8$ and H_2L^5 with ZnL^1. Abscissa coordinates correspond to the log K_{ZnL^1-S} sequence (Table 2). Solvent = 1,2-dichloroethane; T = 25.0(2) °C.

Destabilization of ZnL^1-S1 with respect to $ZnTPP-S1$ results from the constraints exerted by the strap on the tetrapyrrolic macrocycle as well as from the out-of-plane pull of the metal center toward the distal face (~0.3 Å).[15,16] The very small red shifts of the Soret and Q bands (~2 nm) and the unaltered phen absorption bands confirmed the proximal binding of $S1$. The stability sequence, determined within experimental errors, for $ZnTPP$ and the substrates ($S3 > S1 > S8 > S2 > S6 > H_2L^5 > S5 > S7 > S4$) is significantly

altered by the presence of the phen strap in ZnL^1 ($S3 > H_2L^5 > S2 > S6 > S8 > S7-S5 > S1 > S4$) and the nature and bulkiness of the substituents of the substrates. $\pi-\pi$ stacking interactions between the phenyl group of $S4$ and the porphyrin plane of ZnL^1 constitute a relevant example of these secondary, weak interactions (Figure S38 in the Supporting Information). CH$-\pi$ interactions between the methyl substituent of $S3$ or $S7$ and the phenyl spacers of the strap (Figure S38 in the Supporting Information) or $\pi-\pi$ interactions between the benzimidazole planes ($S6$, $S7$, $S8$) and the same phenyl spacers (Figure S39 in the Supporting Information) also contribute to strengthening the corresponding edifices.

Interestingly, a strong stabilization of approximately 2 orders of magnitude of the $ZnL^1-H_2L^6$ bisporphyrin complex with respect to $ZnTPP-H_2L^6$ was observed. This effect was ascribed to $\pi-\pi$ interactions between the phenylethynyl spacer of H_2L^6 and the metalloporphyrin plane of ZnL^1 (Figure 7). These data emphasized that stable self-assembled bisporphyrin edifices could be generated in solution, and that the modeled center-to-center distance of ~13 Å is properly tailored to minimize steric interactions between the two porphyrins (Figure 7).
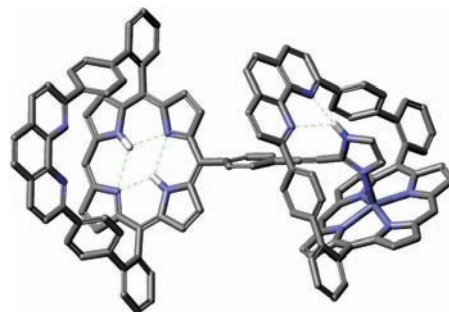
Figure 7. Modeled structure of the bisporphyrin complex $ZnL^1-H_2L^6$ (semiempirical method at the PM3 level). Hydrogen bonds are included as dotted lines.

These thermodynamic parameters highlighted the recognition processes of imidazole substrates by a phen strapped receptor. These parameters showed that the binding led to the formation of two different types of pentacoordinated complexes depending on whether the N_1-pyrrolic nitrogen was substituted or not. A "distal" coordination for the N_1-unsubstituted imidazoles ($S2-S8$, H_2L^5, and H_2L^6) and a "proximal" coordination for the N_1-substituted ones ($S1$) were clearly demonstrated. Receptor ZnL^1 thus exhibits a topography that allows a specific recognition of N_1-unsubstituted imidazoles through a subtle set of a strong N-Zn coordination bond and hydrogen bonds and a panoply of weak interactions (CH$-\pi$ and $\pi-\pi$ stacking interactions).

Coordination of Imidazoles by Strapped−Zn(II)-Porphyrins ZnL^2, ZnL^3, and ZnL^4 with Meso-Substituents. After the characterization of the ZnL^1 complexes with various substrates, the influence of meso-substituents of the strapped porphyrins ZnL^2-ZnL^4 on the recognition properties of imidazoles $S1-S8$ (Figure 2), H_2L^5, and H_2L^6 (Figure 3) was examined. The corresponding spectrophotometric titrations are given in Figures S40−S99 in the Supporting

Information.[22] Regardless of the nature of the substrate and of the receptor, 1:1 pentacoordinated complexes were characterized, in agreement with available structural data.[15,16b] The phen-centered spectroscopic probe was used to establish the proximal or distal coordination. For the meso-substituted receptors (ZnL^2–ZnL^4), the same recognition as for ZnL^1 was observed. These data confirm that the presence of bulky groups (xylyl or 2,6-dimethoxyphenyl) do not alter the distal insertion of the various N_1-unsubstituted imidazoles within the phen cavity. In all cases, except for **S1**, the sizable increase of the stability constants compared with those with Zn**TPP** arises from bifurcated hydrogen bonding between the N_1-H of the substrate and the two nitrogen atoms of the phen moiety. The influence of the meso-substitution on the stability constants was studied by comparing the values obtained for ZnL^2–ZnL^4 and ZnL^1 (Table 2). For ZnL^2–ZnL^4, the complexes formed with N_1-methylated **S1** were further destabilized by a factor of 5–8 in comparison with ZnL^1–**S1**. This destabilization was due to electronic effects and porphyrin ring distortions[50] induced by these meso-substituents.

The thermodynamic data (Table 2) clearly pointed out that the presence of one (ZnL^2) or two (ZnL^3) meso-xylyl substituents had only minor effects on the stability of the corresponding complexes and unexpectedly did not increase significantly the steric hindrance on the distal side as the binding of **S2**–**S8**, H_2L^5, and H_2L^6 remained unchanged. The extensive tilt[15,16b,24] of the phen-strap over the porphyrin plane, the important ruffling of the porphyrin macrocycle,[33,53] and the partial rotation of the xylyl groups toward coplanarity with the porphyrin plane combine to minimize the steric interactions in the inclusion complexes. The main stabilizing interactions (N-Zn coordination bond, bifurcated hydrogen bonds, and π–π and CH–π interactions) are indeed preserved.[15,16b]

In contrast, the presence of 2,6-dimethoxyphenyl meso-substituents had drastic consequences on the association constants (Table 2). The steric hindrance in ZnL^4 forbids the rotation of the 2,6-dimethoxy-phenyl groups toward the porphyrin plane, and thus, the strapped receptor is more sensitive to the bulkiness of the substrate (Figure 8). As a result, the stability constant of ZnL^4–**S4** (log $K_{ZnL4–S4}$ = 2.3(3)) was significantly lowered in comparison to ZnL^1–**S4** (log $K_{ZnL1–S4}$ = 3.92(7)) and ZnL^3–**S4** (log $K_{ZnL3–S4}$ = 4.10(7)) because of the strong steric interactions between the phenyl substituent of **S4** and the ZnL^4 host. Similarly, both bisporphyrin scaffolds ZnL^4–H_2L^5 (log $K_{ZnL4–H2L^5}$ = 5.2(4)) and ZnL^4-H_2L^6 (log $K_{ZnL4–H2L^6}$ = 5.0(3)) were about 1 order of magnitude less stable than the respective complexes with ZnL^1. Thus, the presence of the resorcinol-type substituents inhibits π–π interactions between the metal-

loporphyrin macrocycle and the phenylethnyl spacers of H_2L^5 and H_2L^6.
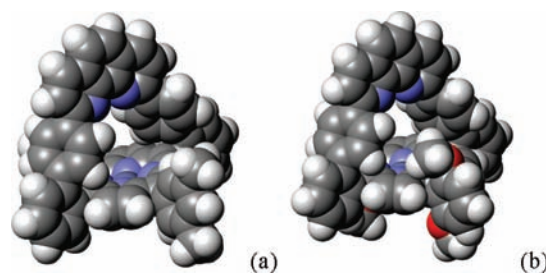
Figure 8. CPK representation of the modeled structures of (a) ZnL^3 and (b) ZnL^4 showing the more hindered binding cavity for ZnL^4 compared with ZnL^3.

It is rather surprising that the steric hindrance contributes to the stabilization of pentacoordinated complexes with small substrates (**S2** and **S3**) and ZnL^4. The changes in the stability within the ZnL^i–**S2** series of complexes ($i = 1$–4) shows that **S2** is stabilized by about 1 order of magnitude upon inclusion in ZnL^4 with respect to its inclusion in receptors ZnL^1–ZnL^3. This higher affinity most likely results from an enhanced inertness due to the meso-resorcinol-type substituents of ZnL^4, which act as "stoppers" (Table 2). Similar increased ligand affinities were previously reported for picket fence heme models[54] and for iron(II) tetramesitylporphyrin[55] compared to iron tetraphenylporphyrin. Traylor has called this type of stabilization effect the "ortho effect".[55]

Recognition Mechanism. Kinetic data on metalloporphyrins are extremely scarce in the literature.[56] Nevertheless these data are essential to both deciphering the assembly mechanism[21] and the understanding of the distal recognition process. Therefore, a kinetic study (absorption and/or emission monitoring) was conducted to decrypt the formation of pentacoordinated species with phen-strapped porphyrin receptors ZnL^1–ZnL^4. Kinetic measurements were carried out under pseudo-first-order conditions using stopped-flow techniques. For 1-methyl-1H-imidazole **S1** (proximal recognition), the reactions were too fast to be measured under our experimental conditions, in agreement with data reported, for instance, for Zn**TPP** and **S2** (log k_f = 9.5 ± 0.5 at 298 K in chlorobenzene).[56,57] For substrates **S3**–**S8**, H_2L^5, and H_2L^6, for which distal binding was clearly demonstrated, the reaction times were slow enough to be recorded with stopped-flow devices. The binding of the smallest substrate **S2** (distal recognition) by ZnL^1–ZnL^4 was too fast to be measured, however.

The presence of the phen strap in ZnL^1–ZnL^4 significantly slows down the formation reactions of the corresponding pentacoordinated complexes, thus rendering the formation kinetics accessible to stopped-flow techniques. A single rate-limiting step was observed with no evidence of slowest or fastest steps (see example provided in Figure 9a).

The pseudo-first-order rate constants k_{obs} (s^{-1}) vary linearly with the concentration of the substrates (Figure 9b and Figures S100–S127 and Tables S1–S28 in the Supporting Information), and the ordinates at the origin were determined with good accuracy. The bimolecular formation rate constants
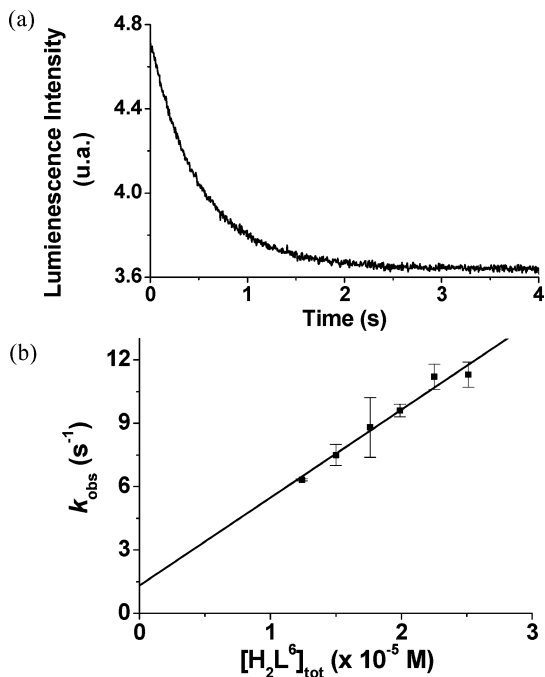
(53) Wondimagegn, T.; Ghosh, A. *J. Phys. Chem. A* **2000**, *104*, 4606–4608.
(54) Collman, J. P.; Brauman, J. I.; Iverson, B. L.; Sessler, J. L.; Morris, R. M.; Gibson, Q. H. *J. Am. Chem. Soc.* **1983**, *105*, 3052–3064.
(55) Portela, C. F.; Madge, D.; Traylor, T. G. *Inorg. Chem.* **1993**, *32*, 1313–1320.
(56) Caldin, E.; Field, J. P. *J. Chem. Soc., Faraday Trans. 1* **1982**, *78*, 1923–1935.
(57) Ware, W. R.; Novros, J. S. *J. Phys. Chem.* **1966**, *70*, 3246–3253.

Figure 9. (a) Variation of the luminescence intensity versus time for the formation of the ZnL^1–H_2L^6 complex. Solvent = 1,2-dichloroethane; T = 25.0(2) °C; l = 1 cm; $[ZnL^1]$ = 4.93 × 10^{-7} M; $[H_2L^6]$ = 1.24 × 10^{-5} M; λ_{exc} = 424 nm; set of band-pass filter (λ > 550 nm) and interference filter (λ < 660 nm). (b) Variation of the pseudo-first-order constants k_{obs} (s^{-1}) for the formation of the ZnL^1–H_2L^6 complex versus $[H_2L^6]_{tot}$. Solvent = 1,2-dichloroethane; T = 25.0(2) °C; $[ZnL^1]$ = 4.93 × 10^{-7} M.

k_f (M^{-1} s^{-1}) and the monomolecular dissociation constants k_d (s^{-1}) are given in Table 3.

Under our experimental conditions, except for **S4**, the sequence of the second-order rate constants k_f for all the receptors examined (ZnL^1–ZnL^4) was as follows: benzimidazoles > substituted imidazoles > porphyrin–imidazoles. Substrate **S4** stands in an interesting contrast, which could be explained by the bulky phenyl group that is very sensitive to meso-substitution of the receptors. Consequently, the largest decrease in k_f (>1.6 orders of magnitude) was observed for ZnL^4–**S4** in comparison with ZnL^1–**S4** (Table 3). For substrates **S3**, **S5**–**S8**, H_2L^5, and H_2L^6, the substitution by one (ZnL^2) or two (ZnL^3) xylyl groups only moderately influenced the k_f values (Table 3). This kinetic property is mainly due to the free rotating nature of the xylyl substituents that keeps the steric constraints to a minimum. The two resorcinol-type substituents bore by ZnL^4 drastically decrease the formation kinetics by about 1 order of magnitude with respect to ZnL^3, especially when steric bulk increases at the 2-position of the imidazole. For the 2-methyl-benzimidazole **S7**, no influence of the meso-substitution was observed in the ZnL^1–ZnL^4 series, whereas an unusual acceleration of the binding reaction rate occurred with **S6** and **S8**. These results could be explained by the rigid and planar structure of these benzimidazole substrates.

The lability of the substituted imidazoles **S3** and **S5** was very sensitive to the presence of steric bulk at the meso-substitution of the zinc porphyrin receptors. For instance, a significant decrease (1–3 orders of magnitude) in inertness was observed for the corresponding ZnL^4 complexes, suggesting that the resorcinol-type meso-substituents act as

efficient "stoppers". Due to their rigid and planar structures, the three benzimidazoles **S6**, **S7**, and **S8** strongly distort the receptors ZnL^1–ZnL^4 and consequently lead to more labile species (Table 3). When the bulkiness of the meso-substituents increases in ZnL^4, the strong steric interactions between 2-phenyl-1H-imidazole **S4** and the 2,6-dimethoxyphenyl groups lead to more labile complexes (Table 3). For the imidazolyl free-base porphyrins H_2L^5 and H_2L^6, no significant variation of the dissociation rate constants k_d was observed in the ZnL^1–ZnL^4 series.

It was demonstrated that the sizable flexibility of the porphyrin receptors favored the distal axial coordination of a wide series of substrates without weakening the main stabilizing interactions (N-Zn coordination and hydrogen bonding). This distal binding, however, induces a significant energetic cost and leads to severe deformations of the porphyrin receptors, especially when bulky meso-substituents are introduced. Kinetic data clearly exemplify this tendency and highlight that when binding requires strong distortion of the receptors because of bulky guests, the resulting assemblies are more labile. The k_d values hence result from a delicate balance between secondary stabilizing interactions (CH–π and π–π) and destabilizing steric interactions and structural deformations of the porphyrin host exerted by bulky substrates.

Activation Parameters. Substrate **S4** exhibited the most interesting kinetic behavior. Therefore, to better understand the self-assembly mechanism, the activation enthalpies and entropies of both the formation and dissociation steps were determined for complexes ZnL^i–**S4** (i = 1–4). As an example, Eyring plots (k_f and k_d) are given in Figure 10 and Figures S128–S135 in the Supporting Information.[22] The activation parameters determined for ZnL^i–**S4** (i = 1–4) are given in Table 4, and relevant data are provided in Tables S29–S36 in the Supporting Information.

Among the four pentacoordinated metalloporphyrins (Table 4), complexes ZnL^1–**S4** and ZnL^4–**S4** represent two distinct examples. ZnL^4 bears bulky resorcinol-type meso-substituents and exhibits similar activation enthalpies for the formation and dissociation of ZnL^4–**S4** ($\Delta H^{\ddagger}_f$ = 74(4) kJ mol^{-1} and $\Delta H^{\ddagger}_d$ = 71(3) kJ mol^{-1}), whereas the activation entropies values are significantly different ($\Delta S^{\ddagger}_f$ = 53(12) J mol^{-1} K^{-1} and $\Delta S^{\ddagger}_d$ = 4(9) J mol^{-1} K^{-1}). Consequently, the binding equilibrium is dissociative and entropically driven with $\Delta\Delta S^{\ddagger}$ = 49(15) J mol^{-1} K^{-1}. On the contrary, the unhindered complex ZnL^1–**S4** possesses activation enthalpies for formation and dissociation ($\Delta H^{\ddagger}_f$ = 42(2) kJ mol^{-1} and $\Delta H^{\ddagger}_d$ = 65(4) kJ mol^{-1}) that suggest an enthalpically controlled equilibrium ($\Delta\Delta H^{\ddagger}$ = −23(2) kJ mol^{-1}). These parameters are completed by $\Delta S^{\ddagger}_f$ = −26.0(9) J mol^{-1} K^{-1} and $\Delta S^{\ddagger}_d$ = −28(2) J mol^{-1} K^{-1}. Thus, in the absence of steric interactions between **S4** and ZnL^1, the binding event proceeds through an associative mechanism with an enthalpic contribution. ZnL^2 binds **S4** via a similar pathway. The assembly mechanism of ZnL^4 with **S4** is dissociative and

(58) (a) Espenson, J. H. In *Chemical Kinetics and Reaction Mechanisms*, 2nd ed.; McGraw-Hill: New York, 1995. (b) Poë, A. J. In *Mechanisms of Inorganic and Organometallic Reactions*; Twigg, M. V., Ed.; Plenum Press: New York, 1994, Vol. 8, Chapter 10.

Table 3. Averaged Rate Constants Determined by Kinetic Studies for the Formation Mechanism of Pentacoordinated Complexes with ZnL^1-ZnL^{4a}

		S3	S4	S5	S6
ZnL^1	k_f (M^{-1} s^{-1})^d	$2.2(9) \times 10^7$	$2.0(7) \times 10^4$	$1.54(8) \times 10^5$	$6.4(8) \times 10^{7d}$
ZnL^2		$1.7(3) \times 10^7$	$1.3(2) \times 10^4$	$5(3) \times 10^5$	nd
ZnL^3		$1.7(7) \times 10^7$	$6.0(2) \times 10^3$	$8(2) \times 10^5$	nd
ZnL^4		$3(2) \times 10^6$	$4.9(1) \times 10^2$	$2.0(3) \times 10^4$	nd
ZnL^1	k_d (s^{-1})^d	$16(8)$	$1.4(2)$	$14(2)$	$162(51)^d$
ZnL^2		$1.7(8)^c$	$0.5(1)$	$11(7)$	nd
ZnL^3		$1.7(8)^c$	$0.44(5)$	$16(9)$	nd
ZnL^4		$0.06(6)^c$	$4.3(3)$	$0.65(9)$	nd

		S7	S8	H_2L^5	H_2L^6
ZnL^1	k_f (M^{-1} s^{-1})^d	$2.5(4) \times 10^{7b}$	$6.3(6) \times 10^{7b}$	$3.2(1.0) \times 10^5$	$4.2(1.0) \times 10^5$
ZnL^2		$3.2(2) \times 10^{7b}$	$2.5(2) \times 10^{7b}$	$2.2(3) \times 10^5$	$2.1(9) \times 10^5$
ZnL^3		$2.0(4) \times 10^{7b}$	$1.4(2) \times 10^{8d}$	$2.3(3) \times 10^5$	$1.7(3) \times 10^5$
ZnL^4		$1.9(6) \times 10^{7b}$	nd	$1.7(6) \times 10^4$	$1.6(2) \times 10^4$
ZnL^1	k_d (s^{-1})^d	$136(21)^b$	$110(35)^b$	$0.24(0.16)$	$1.3(7)$
ZnL^2		$92(11)^b$	$44(3)^b$	$2.3(7)$	$3.0(1.3)$
ZnL^3		$54(20)^b$	$142(42)^b$	$0.5(3)$	$0.5(2)$
ZnL^4		$192(22)^b$	nd	$1.2(3)$	$0.22(7)$

^{a} Solvent = 1,2-dichloroethane; T = 25.0(2) °C. UV−vis absorption and fluorescence kinetic measurements. Uncertainties = 3σ. See ESI for detailed experiments. ^{b} Fluorescence kinetic measurements. ^{c} Estimated values. nd: not accurately determined because of the fast reaction. ^{d} $k_{obs} = k_f[S^n]_{tot} + k_d$.

(a)

(b)
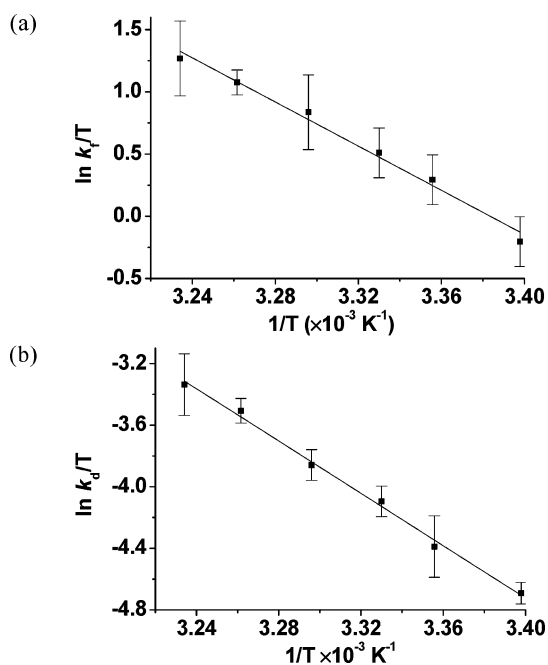
Figure 10. Eyring plots for (a) the formation and (b) the dissociation of ZnL^4-S4 complex. Solvent = 1,2-dichloroethane.

Table 4. Enthalpies and Entropies for the Formation ($\Delta H_f^{\ddagger}$, $\Delta S_f^{\ddagger}$) and the Dissociation ($\Delta H_d^{\ddagger}$, $\Delta S_d^{\ddagger}$) of ZnL^i-S4 Complexes (i = 1−4)^a

	formation		dissociation	
	$\Delta H_f^{\ddagger}$ (kJ mol^{-1})	$\Delta S_f^{\ddagger}$ (J K^{-1} mol^{-1})	$\Delta H_d^{\ddagger}$ (kJ mol^{-1})	$\Delta S_d^{\ddagger}$ (J K^{-1} mol^{-1})
ZnL^1	42(2)	−26(6)	65(4)	−28(12)
ZnL^2	29(2)	−70(6)	72(4)	−4(9)
ZnL^3	35(2)	−54(6)	82(6)	24(18)
ZnL^4	*74(4)*	53(12)	*71(3)*	4(9)

^{a} Solvent = 1,2-dichloroethane. Uncertainties = 3σ with $\sigma(\Delta H^{\ddagger}) \sim \sigma(\Delta S^{\ddagger}) \times 1/T_{av}$.[58]

entropically driven, due to conformational changes of the substrate and to distortions of the receptor. The presence of two xylyl substituents in ZnL^3 significantly alters the energetic profile of both the formation and the dissociation reactions, which are associative and dissociative, respectively. The two meso-xylyl substituents in ZnL^3 do not strongly influence the

entry of substrate **S4** within the receptor's binding cavity; however, they do play a key role in the release pathway.

Self-Assembled Photochemical Dyads. Regardless of the nature of the meso-substituents, the strapped Zn(II) porphyrin receptors (ZnL^1-ZnL^4) are able to self-assemble with the two imidazole-appended free-base porphyrins (H_2L^5 and H_2L^6). In the corresponding dyads, the length of the phenylethynyl spacer (~8 Å) is sufficiently long enough to minimize steric hindrance between the two porphyrins. It is noteworthy that in these photoactive dyads, the strapped Zn(II) porphyrin−imidazole complexes constitute the effective energy donors (or photochemical antenna) and the appended free-base porphyrins play the role of the energy acceptors (Figure 11). The center-to-center distances between the two porphyrins were estimated from molecular mechanics to be ~12.5−13 Å.
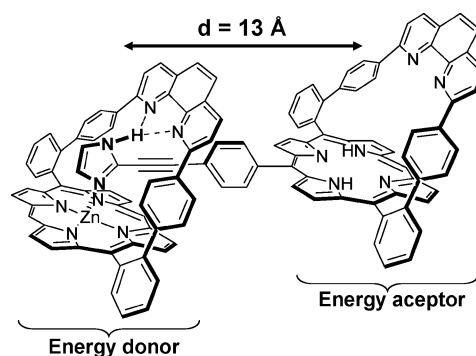
Figure 11. Schematic representation of the bisporphyrin photodyad $ZnL^1-H_2L^6$.

The spectrophotometric properties (Q bands) of the free receptors, of the imidazolyl free-base porphyrins and of the corresponding dyads are given in Table S37 in the Supporting Information. For the sake of comparison, the spectrophotometric data of complexes ZnL^i-S2 (i = 1−4) are also provided (Table S37 in the Supporting Information), because they correspond to the effective energy donors within the corresponding photochemical dyads. Regardless of the nature of the dyads, the ground-state electronic spectra of their Q

bands correspond to the sum of the spectra of the component porphyrins. This observation strongly suggests weak electronic coupling[59] between the two chromophores (Figures S136−S143 in the Supporting Information). These results are also supported by the electrochemical properties obtained for the $ZnL^1−H_2L^5$ complex.[18]

The photophysical properties of the receptors ZnL^i ($i = 1−4$) and of the imidazolyl free-base porphyrins H_2L^5 and H_2L^6 are given in Table 5. The data obtained for $ZnL^i−S2$, which mimic the energy donors in the photochemical dyads, are also reported. The photophysical characteristics of these porphyrins are dependent on the structure, symmetry, and bulkiness of the tetrapyrrolic macrocycle.[41] Indeed, deformation of the porphyrin imposed by the meso-substituents decreases the HOMO and LUMO energy gap and hence results in bathochromic shifts of the $S_1 \rightarrow S_0$ emission bands with respect to the unsubstituted ZnL^1 reference. Furthermore, the constraints induced by the bulky meso-substituents as well as the asymmetrical substitution, such as in ZnL^2, led to a significant decrease of luminescence quantum yield compared with that of ZnL^1 (Table 1).

Table 5. Photophysical Parameters of ZnL^i ($i = 1−4$) Receptors, of H_2L^5 and H_2L^6, and of $ZnL^i−S2$ Pentacoordinated Complexes[a]

compounds	λ_{exc} (nm)	λ^{em}_{max} (nm)		Q_L^{abs} (%)
		Q(0,0)	Q(0,1)	
H_2L^5	421	653	716	3.5
H_2L^6	421	650	712	2.1
ZnL^1	420	594	646	1.6
ZnL^2	422	601	648	0.9
ZnL^3	428	609	659	1.4
ZnL^4	433	611	664	1.5
$ZnL^1−S2$[b]	424	604	657	1.2
$ZnL^2−S2$[b]	429	613	667	0.7
$ZnL^3−S2$[b]	435	622	676	0.9
$ZnL^4−S2$[b]	436	620	674	1.3

[a] Solvent = 1,2-dichloroethane; T = 25.0(2) °C. [b] Calculated from emission titrations of the ZnL^i receptors with the 1H-imidazole S2 substrate. λ_{exc} corresponds either to the maximum of absorption of the Soret band for ZnL^i, H_2L^5, and H_2L^6 or to isosbestic point between ZnL^i and $ZnL^i−S2$. The uncertainties on the λ^{em}_{max} and Q_L^{abs} are 1 nm and 30%, respectively.

The recognition of the imidazolyl free-base porphyrins H_2L^5 and H_2L^6 by ZnL^i ($i = 1−4$) was therefore monitored by spectrofluorimetry (Figure 12). The stability constants obtained were in excellent agreement with those determined in the ground state (Table S38), thus demonstrating that the recognition properties were preserved in the excited state (Table S38 in the Supporting Information). As a representative example, the spectrofluorimetric titration of ZnL^3 by H_2L^5 (Figure 12) clearly shows a drastic decrease of the Zn(II) metalloporphyrin emission band (609 nm) with a concomitant increase of the free-base porphyrin-centered emission bands at 653 and 716 nm (Table 5). The absorption spectra of the strapped zinc porphyrins severely overlapped with those of the free-base porphyrins. This overlap prevented selective excitation of the input unit (i.e., the $ZnL^i−S2$ model of the dyads). In $ZnL^3−H_2L^5$, for example, it is calculated that for an equimolar mixture of both reactants (Figure 12) and at λ_{exc} = 554 nm, ∼86.5% of the incident

(59) Dexter, D. L. *J. Chem. Phys.* **1953**, *21*, 836−850.

excitation light will be absorbed by the Zn(II) porphyrin (66.6% for $ZnL^3−H_2L^5$ and 19.9% for free ZnL^3), whereas ∼13.5% will be absorbed by free H_2L^5. These observations are also valid for the other photodyads and emphasized that our experimental conditions are well set up to monitor the dyad formation by steady-state luminescence spectroscopy and to conclude whether the energy transfer is efficient or not.
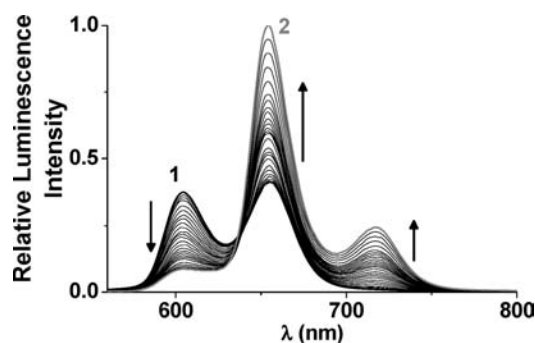
Figure 12. Spectrofluorometric titration of ZnL^3 by H_2L^5. Solvent = 1,2-dichloroethane; T = 25.0(2)°C; $[ZnL^3]_{tot}$ = 1.11 × 10⁻⁵ M; (**1**) $[H_2L^5]_{tot}/[ZnL^3]_{tot}$ = 0; (**2**) $[H_2L^5]_{tot}/[ZnL^3]_{tot}$ = 1.56; λ_{exc} = 554 nm; emission and excitation bandwidths = 10 nm.

As an example, Figure 13 displays the steady-state luminescence emission spectrum of $ZnL^3−H_2L^5$ compared to those of $ZnL^3−S2$ and of H_2L^5. The emission spectrum of the dyad closely resembles that of the free-base porphyrin acceptor, thus substantiating that efficient energy migration occurs within these photoactive edifices. Moreover, a residual emission signal most likely arising from the donor (i.e., the pentacoordinated Zn(II) strapped porphyrin) is also observed and corresponds to the $ZnL^3−S2$ model emission. About 80% of the excitation energy of $ZnL^3−S2$ is transferred to the appended free-base porphyrin H_2L^5 within the corresponding dyad (Tables 5 and 6). The other self-assembled dyads exhibit comparable behavior, with at least 4−10-fold quenching of the zinc porphyrin's emission (Table 6).
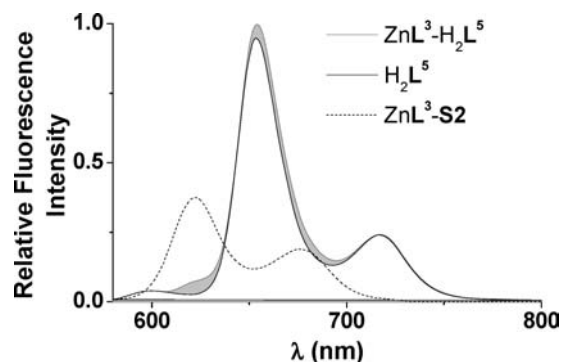
Figure 13. Steady-state fluorescence emission spectra of $ZnL^3−H_2L^5$ (gray line) compared to that of H_2L^5 (black line) and that of the antennae model unit $ZnL^3−S2$ (dotted line). $ZnL^3−S2$ centered emission is quenched, while H_2L^5 centered emission is exalted within the dyad $ZnL^3−H_2L^5$. The area filled in gray corresponds to the nontransmitted emission signal arising from the pentacoordinated Zn(II) porphyrin within the dyad. Solvent = dichloroethane; T = 25.0(2) °C; λ_{ex} = 543 nm.

Modeling Energy Transfer: Förster Approach. Our spectrophotometric results, as well as electrochemical data,[18] clearly indicate the absence of interporphyrin electronic

interactions. Therefore, the possibility of dipole−dipole Förster interactions[60−62] was examined using a steady-state approach. The efficiency of the energy transfer Q_{ET} (eq 1) was estimated from spectrophotometric and photophysical data of the separate donor (ZnL^i−$S2$) and acceptor (H_2L^5 or H_2L^6) entities, using the following equation:
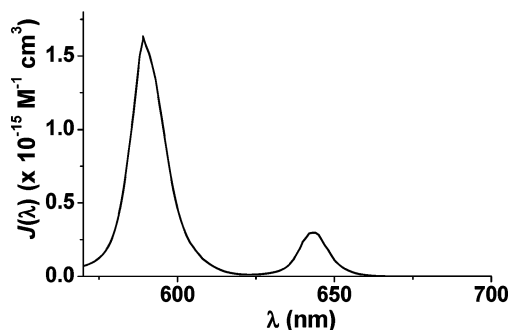
$$Q_{ET} = R_0^6/(R_0^6 + d^6) \qquad (1)$$

where d (∼13 Å) is the donor−acceptor distance that was assumed to be comparable for all dyads, R_0 is the Förster critical radius that is defined as the center-to-center distance between the two fluorophores for which Q_{ET} = 50%.[60,61] The distance R_0 (eq 3) varies with

$$R_0 = 9.78 \times 10^3 [\kappa^2 n^{-4} Q_D J(\lambda)]^{1/6} \qquad (2)$$

where Q_D is the donor's fluorescence quantum yield (Table 5), n is the index of refraction of the medium (n^{25} = 1.4448), and $J(\lambda)$ is the spectral overlap of the fluorescence bands of the donor (ZnL^i−$S2$; i = 1−4) with the absorption bands of the acceptor (H_2L^5 or H_2L^6). The mutual orientation of the donor's and the acceptor's transition moments was estimated[63] to be κ^2 = 0.9 from the PM3 model of the ZnL^1−H_2L^6 dyad (Figure 7). This κ^2 value agrees well with values ($2/3 < \kappa^2 < 1.25$) commonly used in the literature for donor−acceptor pairs similar to those presented in this work.[18,64,65] The spectral overlap integral $J(\lambda)$ (shown in Figure 14 and Figures S144−S151 in the Supporting Information) is calculated from the acceptor's absorption spectrum ($\varepsilon(\lambda)$) and the donor's normalized emission spectrum ($F(\lambda)$) as follows:

$$J = \int_0^\infty \varepsilon(\lambda) \, F(\lambda) \lambda^4 \, d\lambda \qquad (3)$$

The values of the spectral overlap integral $J(\lambda)$, of the Förster critical radius (R_0), and of the estimated energy transfer efficiency (Q_{ET}) are given in Table 6.[60,61] These data clearly reflect the optimization of the photoinduced processes by a large

(60) Förster, T. *Discuss. Faraday Soc.* **1959**, *27*, 7−17.
(61) (a) Förster, T. *Naturwissenschaften* **1946**, *33*, 166−175. (b) Förster, T. *Ann. Phys.* **1948**, *2*, 55−73.
(62) Clegg, R. Fluorescence Resonance Energy Transfer and Nucleic Acids. In *Methods in Enzymology*; Lilley, D. M. J., Dahlberg, J. E., Eds.; Academic Press: San Diego, CA, 1992; Vol. 211, pp 353−388.
(63) Martensson, J. *Chem. Phys. Lett.* **1994**, *229*, 449−456.
(64) Kilsa, K. J.; Kajanus, J.; Martensson, J.; Albinsson, B. *J. Phys. Chem. B* **1999**, *103*, 7329−7339.
(65) (a) Hsiao, J. S. P.; Krueger, B.; Wagner, R. W.; Johnson, T. E.; Delaney, J. K.; Mauzerall, D. C.; Fleming, G. R.; Lindsey, J. S.; Bocian, D. F.; Donohoe, R. *J. Am. Chem. Soc.* **1996**, *118*, 11181−11193. (b) Osuka, A.; Kobyaashi, F.; Maruyama, K.; Mataga, N.; Asashi, T.; Okada, T.; Yamazaki, I.; Nishimura, Y. *Chem. Phys. Lett.* **1993**, *201*, 223−228. (c) Osuka, A.; Maruyama, K.; Yamazaki, I.; Tamai, N. *Chem. Phys. Lett.* **1990**, *165*, 392−396.
(66) Hsio, J. S.; Krueger, B. P.; Wagner, R. W.; Thomas, E. J.; Delaney, J. K.; Mauzerall, D. C.; Fleming, G. R.; Lindsey, J. S.; Bocian, D. F.; Donohoe, R. J. *J. Am. Chem. Soc.* **1996**, *118*, 11181−11193.
(67) Kilsa, K. J.; van Berlekom, S. B.; Kajanus, J.; Martensson, J.; Albinsson, B. *J. Phys. Chem. A* **1997**, *101*, 2218−2220.
(68) Hindin, E.; Kirmaier, C.; Diers, J. R.; Tomizaki, K. Y.; Taniguchi, M.; Lindsey, J. S.; Bocian, D. F.; Holten, D. *J. Phys. Chem. B* **2004**, *108*, 8190−8200.
(69) Our work: solvent = 1,2-dichloroethane; *T* = 25.0(2) °C; λ_{ex} = 590 nm; λ_{em} = 650 nm.

Figure 14. Spectral overlap integral $J(\lambda)$ for ZnL^1−$S2$ and H_2L^6. Solvent = 1,2-dichloroethane; T = 25.0(2) °C.

spectral overlap between the emission and absorption spectra of the donors and of the acceptors, respectively. The values of the spectral overlap integrals $J(\lambda)$ (1.27×10^{-13} M^{-1} cm^3 < $J(\lambda)$ < 7.44×10^{-13} M^{-1} cm^3 (Figures S144−S151 in the Supporting Information) are consistent with literature values for covalent porphyrin polyads.[64,66−68] The Förster critical distances (24.4 Å < R_0 < 34.2 Å) indicated that the distance (d ∼ 13 Å)[18] between the two chromophores is suitable for quantitative energy transfer (Q_{ET} ≫ 95%).

Table 6. Spectral-Overlap Integrals $J(\lambda)$, Förster Critical Radii (R_0), and Experimental[b] and Estimated[c] Efficiencies of the Energy Transfers for the $ZnL^i \rightarrow H_2L^j$ Dyads (i = 1−4; j = 5, 6)[a]

donor	acceptor	$J(\lambda) \times 10^{13}$ (M^{-1} cm^3)	R_0 (Å)	Q_{ET}[b] experimental	Q_{ET}[c] estimated
ZnL^1−$S2$	H_2L^5	7.4	34.2	91	99.7
	H_2L^5		24.7[d]		97.8[d]
	H_2L^6	2.8	29.1	89	99.3
ZnL^2−$S2$	H_2L^5	6.1	30.3	86	99.5
	H_2L^6	1.8	24.7	92	98.3
ZnL^3−$S2$	H_2L^5	5.2	30.7	80	99.5
	H_2L^6	1.3	24.4	80	98.1
ZnL^4−$S2$	H_2L^5	5.5	33.0	88	99.7
	H_2L^6	1.4	26.3	78	98.8

[a] Solvent = 1,2-dichloroethane; T = 25.0(2) °C. [b] Q_{ET} = $1 - Q_{DA}/Q_D$, where Q_{DA} is the quantum yield of the donor in the dyad and Q_D is the quantum yield of complex ZnL^i−$S2$. [c] Calculated from eq 2 with d = 13 Å. [d] From reference 18 with d = 12.6 Å (see eq 1) and k^2 = 1 (see eq 2). The uncertainty of the Q_{ET} is 10%.

In dyad ZnL^1−H_2L^5, the existence of energy back-transfer from H_2L^5 to ZnL^1 was previously demonstrated.[18] To test the feasibility of an energy back-transfer from H_2L^6 to the penta-coordinated metalloporphyrin within the $H_2L^6 \rightarrow ZnL^1$ system, the corresponding critical Förster radius R'_0 ($J'(\lambda)$ = 1.23×10^{-13} M^{-1} cm^3 and R'_0 = 27.8 Å) was calculated. These data emphasized that the back-transfer process is theoretically efficient too (Q_{ET-1} = 99.1%). This back-transfer may explain the differences in the values of Q_{ET} presented in Table 6. By considering the ZnL^1−H_2L^6 system and the lifetimes τ_{H2L6} (8.99(5) ns)[69] and $\tau_{ZnL1-S2}$ (1.80(3) ns),[18] we determined k_{ET} and k_{ET-1} values (k_{ET} = $(\tau_{ZnL1-S2})^{-1} \times (R_0/d)^6$ = 6.99×10^{10} s^{-1}; k_{ET-1} = $(\tau_{H2L6})^{-1} \times (R'_0/d)^6$ = 1.06×10^{10} s^{-1}) (Figure 15). These dynamic parameters show that among the numerous radiative and nonradiative routes possible in our photodyads, the $ZnL^1 \rightarrow H_2L^6$ energy transfer dominates the photoinduced processes.
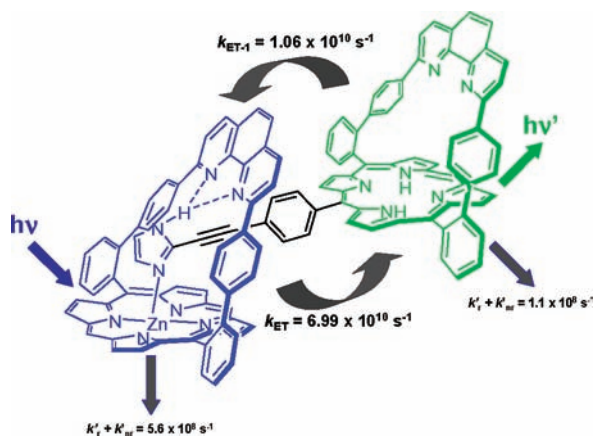
Figure 15. Dynamic processes in $ZnL^1-H_2L^6$ photoactive self-assembled dyad.

Conclusion

The phen-strapped Zn(II) porphyrin receptors ZnL^i ($i = 1-4$) exhibit suitable topography tailored to strongly and selectively bind various N_1-unsubstituted imidazole-type substrates ($S2-S8$) and imidazoles appended with free-base porphyrins (H_2L^5 and H_2L^6). The distal discrimination of imidazole N-Zn axial binding is imposed by the possibility of bifurcated hydrogen bonds with the phenanthroline moiety of the receptors. This property consequently stabilizes the corresponding complexes and leads to an efficient multipoint host−guest system. An extensive physicochemical approach indicated that the introduction of xylyl substituents (ZnL^2, ZnL^3) has little influence on the stability and kinetics of the targeted supramolecules. Xylyl groups do not provide significant steric hindrance around the distal binding of $S2-S8$, H_2L^5, and H_2L^6. Indeed, the sizable flexibility of the receptors and the free rotation of the xylyl substituents toward the porphyrin plane constitute structural features which drastically diminish the steric interactions in the recognition process. For the ZnL^1-ZnL^3 series, the stabilizing interactions (N-Zn coordination bond, bifurcated hydrogen bonds, and $\pi-\pi$ and $CH-\pi$ interactions) are preserved. In contrast, meso-substitution with resorcinol-type moieties (ZnL^4) strikingly led to a host that was much more sensitive to the bulkiness of the substrate due to the inhibited rotation of these moieties. For ZnL^4, the most remarkable outcome concerns the stabilization of the complexes with the smallest substrates ($S2$, $S3$).

The self-assembly mechanism was fully elucidated and supported the conclusions deduced from the equilibrium studies. The presence of the xylyl units does not significantly influence the formation kinetics, whereas resorcinol-type substituents in ZnL^4 drastically slow down the formation kinetics, particularly for 2-substituted substrates. The most important effect was observed when bulkiness was introduced both at the imidazole 2-position ($S4$) and the receptor's meso-positions (ZnL^4). In comparison with ZnL^1-ZnL^3, the inertness of the pentacoordinated ZnL^4 complexes was considerably increased for the smallest substrates ("ortho effect"), whereas more labile species were produced when substrates with bulky 2-substituents were combined.

The determination of the activation parameters with the representative substrate $S4$ provided deeper insight into the self-assembly mechanism. These parameters revealed that bulky ortho substituents in ZnL^4 induced important steric constraints, which were reflected by the associative and enthalpic character of the binding process. For ZnL^1 and ZnL^2, the coordination was dissociative, entropically driven and highlighted weak conformational constraints.

The photoinduced energy migration pathways within the photoactive dyads have been clearly established and quantified. Dipole−dipole interactions between the two porphyrin cores were demonstrated. Experimental data derived from luminescence titrations confirmed that, upon excitation of the metalloporphyrin, excited-state energy migrations occurred efficiently, regardless of the number and the nature of the meso-substituents. However, contrary to models, Q_{ET} values were attenuated because of possible back-transfer processes. Dynamic parameters showed that energy transfer from the pentacoordinated input to the free-base porphyrin output was strongly favored and very efficient. This work provided a basis for the development of multiporphyrin arrays with predictable electronic and photophysical properties. The noncovalent molecular edifices examined in this work revealed to be very efficient photoactive systems, even compared with covalent analogues.

Supporting Information Available: Spectrophotometric titrations (absorption and emission) of the ZnTPP receptor by substrates $S1-S8$ (Figures S1−S16). Spectrophotometric titrations (absorption and emission) of the ZnL^1 receptor by substrates $S1-S8$, H_2L^5, and H_2L^6 (Figures S17−S36). Electronic spectra of 2,9-diphenyl-1,10-phenanthroline and its protonated species (Figure S37). X-ray crystal structures of pentacoordinated Zn(II)−porphyrin complexes (Figures S38−S39). Spectrophotometric titrations (absorption and emission) of the ZnL^2 receptor by substrates $S1-S8$, H_2L^5, and H_2L^6 (Figures S40−S99). Kinetic studies of receptor ZnL^1 (Tables S1−S8 and Figures S100−S107), of receptor ZnL^2 (Tables S9−15 and Figures S108−S114), of receptor ZnL^3 (Tables S16−S22 and Figures S115−S121), and of receptor ZnL^4 (Tables S23−S28 and Figures S122−S127). Activation parameters for ZnL^1-S4 (Tables S29−S30 and Figures S128−S129), for ZnL^2-S4 (Tables S31−S32 and Figures S130−S131), for ZnL^3-S4 (Tables S33 and S34 and Figures S132 and S133) and for ZnL^4-S4 (Tables S35 and S36 and Figures S134 and S135). Spectrophotometric parameters of the porphyrin receptors, substrates, and complexes (Table S37). Stability constants of the bisporphyrin dyads (Table S38). Comparison of the electronic spectra of the dyads with the sum of the electronic spectra of their components (Figures S136−S143). Spectral overlap integrals (Figures S144−S151). This material is available free of charge via the Internet at http://pubs.acs.org.

IC802407X